Brain-wide functional architecture remodeling by alcohol dependence and abstinence

Adam Kimbrough[a] ⓘ, Daniel J. Lurie[b], Andres Collazo[c], Max Kreifeldt[d], Harpreet Sidhu[d], Giovana Camila Macedo[d], Mark D'Esposito[b], Candice Contet[d], and Olivier George[a,1]

[a]Department of Psychiatry, School of Medicine, University of California San Diego, La Jolla, CA 92093; [b]Helen Wills Neuroscience Institute, University of California, Berkeley, CA 94720; [c]Beckman Institute, California Institute of Technology, Pasadena, CA 91125; and [d]Department of Molecular Medicine, The Scripps Research Institute, La Jolla, CA 92037

Alcohol abuse and alcohol dependence are key factors in the development of alcohol use disorder, which is a pervasive societal problem with substantial economic, medical, and psychiatric consequences. Although our understanding of the neurocircuitry that underlies alcohol use has improved, novel brain regions that are involved in alcohol use and novel biomarkers of alcohol use need to be identified. The present study used a single-cell whole-brain imaging approach to 1) assess whether abstinence from alcohol in an animal model of alcohol dependence alters the functional architecture of brain activity and modularity, 2) validate our current knowledge of the neurocircuitry of alcohol abstinence, and 3) discover brain regions that may be involved in alcohol use. Alcohol abstinence resulted in the whole-brain reorganization of functional architecture in mice and a pronounced decrease in modularity that was not observed in nondependent moderate drinkers. Structuring of the alcohol abstinence network revealed three major brain modules: 1) extended amygdala module, 2) midbrain striatal module, and 3) cortico-hippocampo-thalamic module, reminiscent of the three-stage theory. Many hub brain regions that control this network were identified, including several that have been previously overlooked in alcohol research. These results identify brain targets for future research and demonstrate that alcohol use and dependence remodel brain-wide functional architecture to decrease modularity. Further studies are needed to determine whether the changes in coactivation and modularity that are associated with alcohol abstinence are causal features of alcohol dependence or a consequence of excessive drinking and alcohol exposure.

iDISCO | network analysis | graph theory | Fos | dependence

Alcohol abuse and alcohol dependence are key factors in the development of alcohol use disorder, which is a pervasive societal problem with substantial economic, medical, and psychiatric consequences (1). Alcohol dependence can be associated with severe liver and pancreatic diseases that require a need to manage alcohol consumption, which may be greatly aided by increasing our understanding of how a history of moderate alcohol use compared with alcohol dependence and abstinence changes the brain (2). Our knowledge of the neurocircuitry that underlies alcohol use, dependence, and abstinence has improved over the last decade (3, 4), but most preclinical research has focused on only a handful of brain regions of interest because of technical and conceptual limitations. This is a major hurdle for the field because it prevents the discovery of novel brain regions that may be involved in alcohol dependence, limits our ability to discover biomarkers and predictive traits of future alcohol use, and hampers the development of novel approaches for the treatment of alcohol use disorder (5, 6). Moreover, research on brain disorders, such as dementia, seizures, and traumatic brain injury, has revealed global adaptations of the whole-brain functional network, including lower modularity (7–12), and similar effects may be critical for our understanding of alcohol dependence. The present study used a single-cell whole-brain im-

aging approach to 1) assess whether abstinence from alcohol significantly alters the functional architecture of brain activity and leads to changes in modularity, 2) validate our current knowledge of the neurocircuitry of alcohol abstinence, and 3) discover brain regions that may be involved in alcohol dependence and abstinence.

Because of technical limitations, visualizing changes throughout the whole brain at single-cell resolution in rodents that are dependent on alcohol has not previously been possible. However, novel whole-brain imaging approaches, such as CLARITY, immunolabeling-enabled three-dimensional (3D) imaging of solvent cleared organs (iDISCO), ultimate DISCO (uDISCO), and others (13–17), have provided opportunities to expand our knowledge of functional neural circuitry in animal models of alcohol dependence in an unbiased manner. The present study generated a single-cell-resolution, whole-brain atlas of changes in modularity and functional connectivity that were produced by abstinence from alcohol in animal models of alcohol drinking and alcohol dependence using unbiased single-cell whole-brain imaging. We further characterized the alcohol abstinence network to assess hub brain regions that may drive network function and predict alcohol drinking and abstinence-related behaviors. Finally, we assessed modular organization of the alcohol abstinence network compared with brain regions that are proposed to be critical in alcohol dependence (3, 4).

Significance

Visualizing functional changes in brain networks that are produced by alcohol use and alcohol dependence is a critical step in our understanding of the consequences of drinking alcohol. Because of technical limitations, visualizing changes throughout the whole brain at single-cell resolution has not been possible. The present study used a single-cell whole-brain imaging approach in mice to assess whether alcohol abstinence alters functional architecture of the brain. Compared with nondrinkers and casual drinkers, alcohol-dependent mice exhibited widespread increases in coordinated brain activity during abstinence and a decrease in modularity. We also identified target brain regions for future research and provide a single-cell whole-brain atlas that may be used to better understand the consequences of alcohol use, dependence, and abstinence.

www.manaraa.com

NEUROSCIENCE
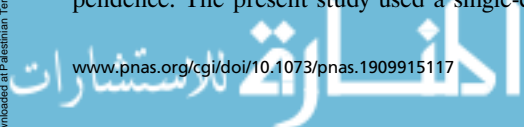
Fig. 1. Experimental design. The mice underwent the 2BC/CIE paradigm. The 2BC/CIE paradigm involves alternating weeks of 2BC (highlighted in blue) and CIE/Air (highlighted in red and gray, 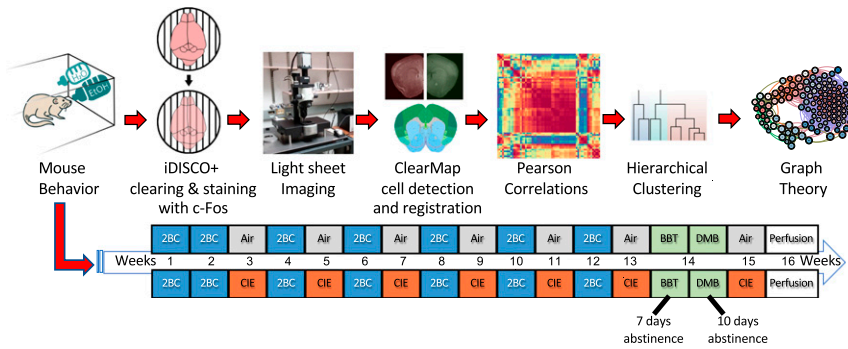respectively). The mice underwent 2 wk of baseline 2BC testing followed by five rounds of alternating CIE or Air weeks and 2BC weeks. The mice then underwent a sixth week of CIE/Air and were then tested for irritability-like and digging behaviors 7 and 10 d, respectively, into abstinence (highlighted in green). The mice then underwent one additional week of CIE/Air, and brains were collected 7 d after the last vapor exposure with no intervening behavioral testing. Brains were collected during the time of day that the mice would normally undergo a 2BC session. Brains were then immunostained for Fos and cleared using the iDISCO+ procedure. Brains were then imaged and analyzed to identify brain regions that potentially contribute to behaviors and the functional networks for each treatment. Key brain regions in the alcohol abstinence network were then identified using graph theory. BBT, bottle-brush test of irritability-like behavior; DM, digging and marble burying.

Results

Experimental Overview. We used a well-validated mouse model of alcohol dependence, the two-bottle choice (2BC)/chronic intermittent ethanol (CIE) vapor paradigm (18), to explore the relationship between behavioral and neural effects of alcohol abstinence. We assessed alcohol intake in alcohol-dependent (2BC/CIE) and nondependent (2BC/Air) mice and assessed irritability-like behavior and digging behavior in 2BC/CIE, 2BC/Air, and alcohol-naive mice. We also identified functional coactivation networks during alcohol abstinence in alcohol-dependent mice and compared them to networks from alcohol-nondependent and naive mice. We then examined changes in modular structuring of the brain that are caused by alcohol abstinence and identified key brain regions that may drive network function. For an experimental outline see Fig. 1.

Alcohol Dependence Escalates Voluntary Alcohol Consumption. After 2 wk of baseline alcohol drinking and five rounds of alternating weeks of 2BC/CIE exposure, alcohol-dependent mice exhibited an increase in drinking compared with nondependent mice that had similar access to drinking but no exposure to alcohol vapor. The repeated-measures ANOVA, with group (alcohol-dependent and nondependent) as the between-subjects factor and week (baseline and postvapor intake) as the within-subjects factor, revealed a significant week × group interaction ($F_{1,7} = 13.9$, $P < 0.05$) and a significant effect of group ($F_{1,7} = 10.0$, $P < 0.05$). The Student–Newman–Keuls (SNK) post hoc test revealed that alcohol-dependent mice significantly escalated their alcohol intake during postvapor week 5 vs. their own baseline (2.8 ± 0.2 g·kg^{-1}·2 h^{-1} at baseline vs. 3.7 ± 0.3 g·kg^{-1}·2 h^{-1} at postvapor week 5), and alcohol-dependent mice had significantly higher alcohol intake compared with nondependent mice at postvapor week 5 (3.7 ± 0.3 g·kg^{-1}·2 h^{-1} for alcohol-dependent vs. 2.3 ± 0.2 g·kg^{-1}·2 h^{-1} for nondependent at postvapor week 5; Fig. 2*A*).

Alcohol Dependence Results in Affective Dysfunction during Abstinence. To evaluate affective dysfunction during alcohol abstinence, we measured irritability-like behavior and digging/marble-burying behavior. Increases in irritability and digging are key symptoms of alcohol abstinence in rodents (19–21). Nondependent mice and naive mice did not differ from each other in total irritability-like behavior scores (60.8 ± 3.4 for nondependent vs. 58.6 ± 3.2 for naive; $t = 0.47$, $P > 0.05$). Therefore, we combined nondependent and naive mice into a

single control group. We found a significant increase in irritability-like behavior 1 wk into abstinence in alcohol-dependent mice compared with control mice (75.3 ± 2.8 for alcohol-dependent vs. 59.7 ± 2.2 for control; $t = 3.92$, $P < 0.005$; Fig. 2*B*). The alcohol-dependent mice also exhibited a significant increase in irritability-like behavior compared with both nondependent mice and naive mice when analyzed as separate groups by one-way ANOVA ($F_{2,11} = 7.3$, $P < 0.05$; *SI Appendix*, Fig. S1*A*).

Similar to irritability-like behavior, nondependent and naive mice did not significantly differ from each other in their composite digging behavior (-0.70 ± 0.25 for nondependent vs. -0.26 ± 0.14 for naive; $t = 1.5$, $P > 0.05$). Therefore, we combined nondependent and naive mice into a single control group. Alcohol-dependent mice exhibited a significant increase in digging behavior
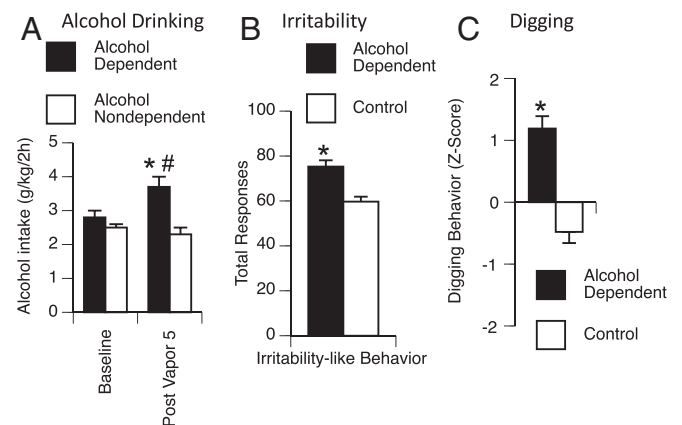

Fig. 2. Alcohol drinking and abstinence behavior in alcohol-dependent vs. control mice. (*A*) Alcohol-dependent mice (black bars) exhibited a significant increase in alcohol drinking during postvapor week-5 2BC testing compared with alcohol drinking in nondependent mice (white bars) and their own baseline intake. (*B*) Irritability-like behavior. Alcohol-dependent mice (black bar) exhibited a significant increase in total irritable-like responses compared with control mice (nondependent and naive; white bar). (*C*) Digging behavior. Alcohol-dependent mice (black bar) exhibited a significant increase in composite digging behavior (Z-score of digging behaviors) compared with control mice (nondependent and naive; white bar). *$P < 0.05$ (two-tailed), alcohol-dependent vs. nondependent for alcohol drinking or control for irritability-like and digging behavior; #$P < 0.05$ (two-tailed), alcohol-dependent postvapor week 5 vs. alcohol-dependent baseline.
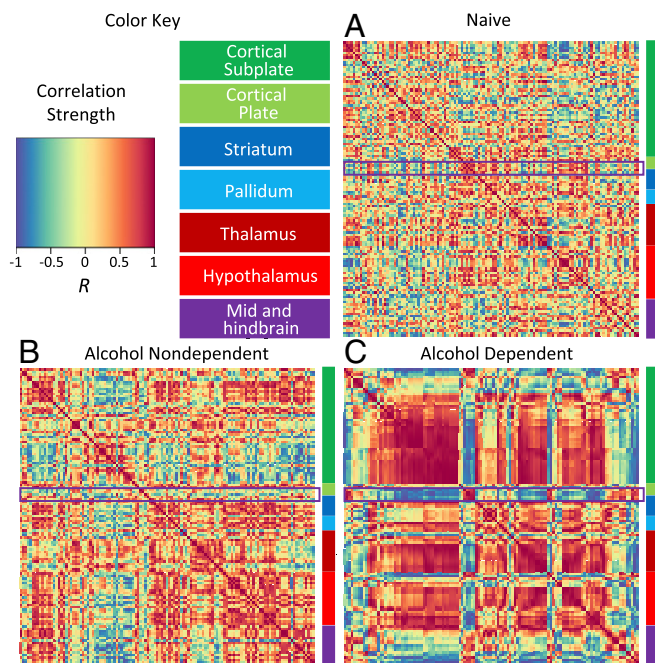
www.manaraa.com

Fig. 3. Interbrain regional Pearson correlation heat maps for each treatment organized anatomically based on the Allen Mouse Brain Atlas. (*A*) Correlation heat map for naive mice. (*B*) Correlation heat map for alcohol-nondependent mice. (*C*) Correlation heat map for alcohol-dependent mice. Each heat map is organized into color-coded anatomical groups: dark green (cortical plate), light green (cortical subplate), dark blue (striatum), light blue (pallidum), dark red (thalamus), light red (hypothalamus), and purple (midbrain, hindbrain, and cerebellum). The region that is highlighted in purple on each heat map represents an amygdala cluster of the heat map that is shown in greater detail in Fig. 4.

1 wk into abstinence compared with control mice (Z score = 1.19 ± 0.20 for alcohol-dependent vs. −0.48 ± 0.18 for control; t = 6.03, P < 0.0005; Fig. 2C). The alcohol-dependent mice also exhibited a significant increase in digging behavior compared with both nondependent and naive mice when analyzed as separate groups by one-way ANOVA ($F_{2,11}$ = 21.7, P < 0.0005; *SI Appendix*, Fig. S1B).

A separate cohort of alcohol-dependent, nondependent, and naive mice was tested for saccharin preference to measure signs of anhedonia, a clinically relevant sign of major depressive disorder (22). We found no significant differences in saccharin intake among groups (*SI Appendix,* Fig. S2), indicating that alcohol-dependent mice did not exhibit an increase in signs of anhedonia.

Identification of Large-Scale Changes in Functional Neural Coactivation Caused by Alcohol Abstinence. To examine whether alcohol use and dependence resulted in changes in brain activity and organization, we examined changes in neural coactivation of the brain and modular structuring that were caused by alcohol abstinence. We first visualized interregional Fos correlations for each treatment condition (alcohol-dependent, nondependent, and naive). Correlation matrices were organized according to traditional anatomical groups from the Allen Mouse Brain Atlas (see Fig. 3, *SI Appendix*, Table S1, and *Materials and Methods* for the order in which brain regions are listed). When visualized this way, clear differences were observed in coactivation patterns between alcohol-dependent mice and nondependent and naive control mice (Fig. 3 A–C). Overall, alcohol-dependent mice exhibited a higher level of cross-correlation between brain regions compared with the control conditions (nondependent and naive). Additionally, nondependent drinkers exhibited moderately higher

levels of cross-correlation between brain regions compared with nondrinkers (naive). However, one cluster of brain regions that included the lateral amygdala (LA), endopiriform nucleus (EP), basolateral amygdala (BLA), central nucleus of the amygdala (CEA), and intercalated amygdala (IA) was notable because it was anticorrelated with most of the other brain regions (framed in Fig. 3 A–C). To further identify the way in which this amygdala cluster is functionally connected to the rest of the brain, we compared correlation patterns of the amygdala cluster with the brain regions that exhibited the highest levels of correlation/anticorrelation by calculating the average correlation across each brain region group (Fig. 4 A and B). A significant effect of group was found in all comparisons of the amygdala cluster to the other clusters that were examined: amygdala cluster intracluster (i.e., amygdala vs. amygdala comparison) correlation (excluding self-correlations; $F_{2,12}$ = 93.8, P < 0.005), cortical amygdala/retrohippocampal cluster (cortical amygdalar nucleus posterior part [COAp], entorhinal area medial part [ENTm], entorhinal area lateral part [ENTl], and parasubiculum; $F_{2,12}$ = 13.5, P < 0.005), parasubthalamic nucleus/tuberal nucleus (PSTN/TU; $F_{2,12}$ = 14.0, P < 0.005), cortical cluster (orbitofrontal cortex [OFC], prefrontal cortex [PFC], and sensory/somatosensory cortex; $F_{2,12}$ = 34.1, P < 0.005), hippocampal cluster (HIPP; fields CA1, CA2, CA3, and dentate gyrus; $F_{2,12}$ = 23.2, P < 0.005), thalamic cluster (THAL; major thalamic nuclei; $F_{2,12}$ = 8.6, P < 0.005), hypothalamic cluster (HYPO; major hypothalamic nuclei; $F_{2,12}$ = 35.0, P < 0.005), and interpeduncular nucleus (IPN) and ventral tegmental area (VTA; $F_{2,12}$ = 4.0, P < 0.05; Fig. 4B). In each instance, the effect of group was driven by the alcohol-dependent group. Interestingly, the cortical amygdala/retrohippocampal and PSTN/TU regions were positively correlated with the amygdala group, whereas the other regions were negatively correlated. These data indicate that alcohol-dependent drinkers presented a major increase in coordinated activity throughout the brain during abstinence
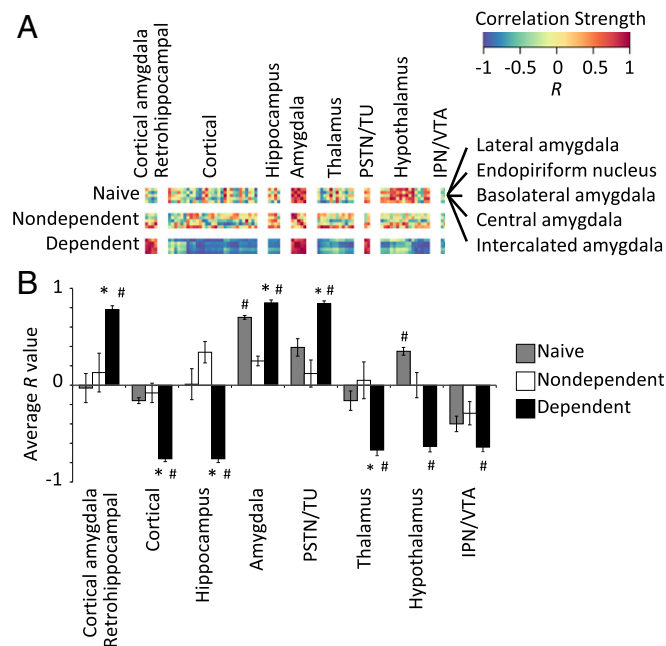
Fig. 4. Comparison of Pearson correlations of an amygdala cluster vs. other regions. (*A*) Cutout of correlations from Fig. 3 of brain regions compared with the amygdala cluster for each treatment. Individual region names are displayed at the bottom, and group names are displayed above each cluster. (*B*) Average R values for alcohol-dependent (black bars), alcohol-nondependent (white bars), and naive (gray bars) mice for each cluster vs. the amygdala cluster. *P < 0.05, vs. naive; #P < 0.05, vs. alcohol-nondependent.

Kimbrough et al.

compared with moderate drinkers and nondrinkers and that moderate drinkers presented a small increase in coordinated activity compared with nondrinkers.

Alcohol Abstinence Results in a Decrease in Modular Structuring of the Brain. Substantial decreases in brain modularity have been observed in such brain disorders as dementia and after traumatic brain injury (7–12), but unclear is whether alcohol dependence results in similar changes in modular organization of the brain. We used hierarchical clustering to identify modular organization of the brain in alcohol-dependent and naive control mice. In control animals, we found that the brain was organized into 9 modules (nondependent drinkers) and 10 modules (naive mice), indicating a modest decrease in modularity in nondependent drinkers. Interestingly, alcohol abstinence resulted in only three large modules, indicating an overall decrease in modularity (Fig. 5). In the controls (nondependent and naive),

each individual module consisted of a smaller subset of brain regions compared with modules in alcohol-dependent mice. Notably, the decrease in the number of modules that was caused by alcohol abstinence compared with the other groups was independent of the clustering thresholds that were used (Fig. 5D).

In the alcohol-dependent network, hierarchical clustering identified two modules with opposing coactivation patterns and a third module that showed moderate coactivation with each of the other modules. We named the modules in the alcohol-dependent network based on the predominant regional components within each module (e.g., regions with the highest intramodule connectivity). One module was an extended amygdala module (module A), consisting of the CEA, BLA, LA, and IA. This module also contained the gustatory area (GU), PSTN, and medial habenula (MH), among other regions. A second module was a midbrain striatal module (module B), which consisted of the periaqueductal gray (PAG), paraventricular thalamus (PVT),
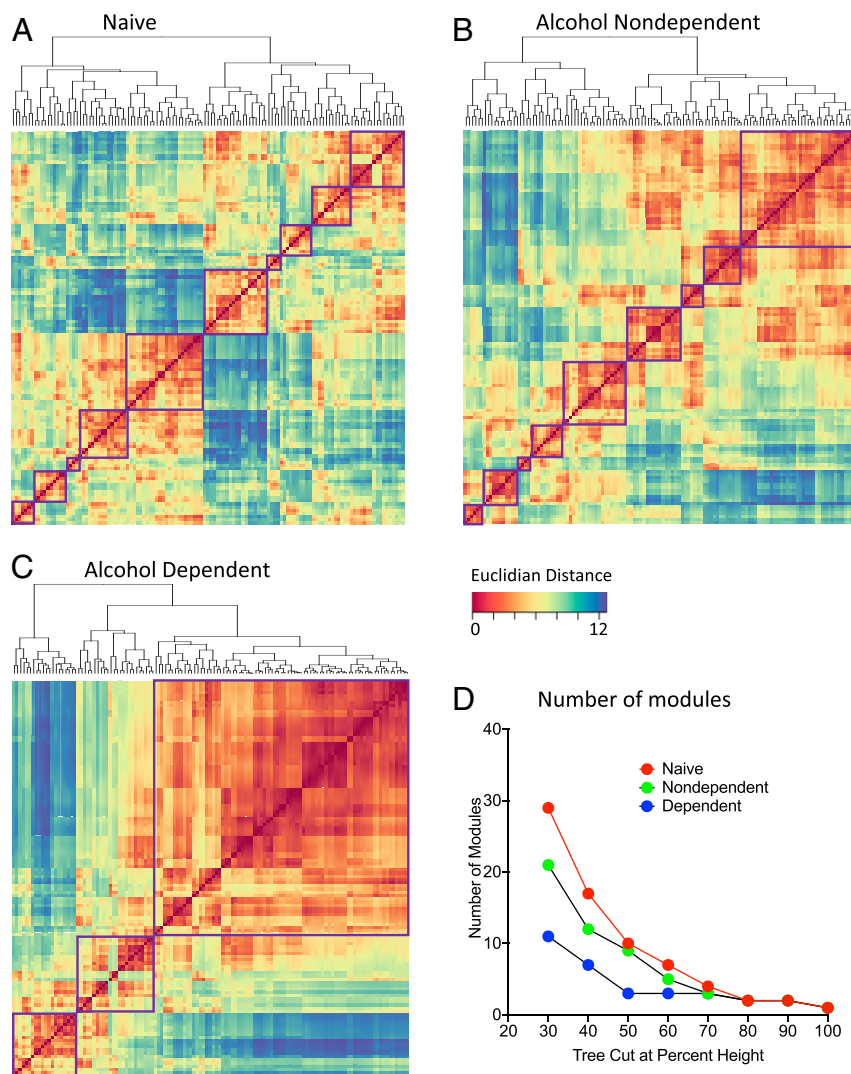

Fig. 5. Hierarchical clustering of complete Euclidean distance matrices for each treatment. Modules were determined by cutting each dendrogram at half of the maximal tree height. (*A*) Relative distance of each brain region relative to the others that were examined in naive mice. In naive mice, nine distinct modules of coactivation were identified. (*B*) Relative distance of each brain region relative to the others that were examined in alcohol-nondependent mice. In alcohol-nondependent mice, eight distinct modules of coactivation were identified. (*C*) Relative distance of each brain region relative to the others that were examined in alcohol-dependent mice. In alcohol-dependent mice, three distinct modules of coactivation were identified. For all distance matrices, each module is boxed in purple. (*D*) Number of modules in each treatment condition after cutting the hierarchical clustered dendrogram at different percentages of tree height. In all cases (except at extreme cutoff values; e.g., 70–100%), the alcohol-dependent network showed a lower number of modules compared with the alcohol-nondependent and naive networks.

Kimbrough et al.

www.manaraa.com

pons, substantia nigra reticular and compact (SNr and SNc), midbrain reticular nucleus (MRN), and some additional amygdala areas that were not found in the extended amygdala module. The third module was a cortico-hippocampo-thalamic module (module C) that was highly anticorrelated with the extended amygdala module. The cortico-hippocampo-thalamic module included the PFC, the OFC, sensory and somatosensory cortices, the HIPP, the THAL, and the HYPO. This module also contained the VTA, IPN, lateral habenula (LH), bed nucleus of the stria terminalis (BST), and nucleus accumbens (ACB; Fig. 5C and see *SI Appendix*, Table S1 for a full list of regions and modules). These data indicate that alcohol-dependent drinkers presented a decrease in modular structuring of the brain that was indicative of major structural reorganization of the neural network.

Identification of Key Brain Regions Associated with Alcohol Abstinence. To further characterize the functional network that is associated with alcohol abstinence, we used a graph theory approach to identify potentially critical hub brain regions (i.e., regions with the most intramodule or intermodule connectivity) which may drive activity within the network. We examined positive connectivity (thresholded to functional connections with a Pearson correlation coefficient >0.75 [0.75R] for inclusion as a network connection) of the network that is associated with alcohol abstinence in alcohol-dependent mice using the modules that were identified with hierarchical clustering to partition the regions of the network. The 0.75R threshold was chosen because all of the brain regions in each network showed connections to other regions at this threshold. Previous animal model studies used various thresholds, ranging from 0.3R to 0.85R (23, 24), to examine connectivity. Negative network connectivity was not examined herein because the precise meaning of such connectivity is controversial and thus is not often examined in network-based approaches (25–28).

We determined the participation coefficient (PC; i.e., a measure of importance for intermodule connectivity) and the within-module degree Z-score (WMDz; i.e., a measure of importance for intramodule connectivity) (29) for all brain regions in the network (see *SI Appendix*, Table S1 for a full list of values). We focused on potential hub regions from the extended amygdala module and its direct connections, given the importance of the extended amygdala in the hierarchical clustering analysis (Fig. 5C). In the extended amygdala module, several brain regions had both high PC and high WMDz values (Fig. 6). These regions included the CEA, IA, and superior colliculus sensory related (SCs). Additionally, the posterior cortical amygdala (COAp), PSTN, BLA, and EP had high WMDz values. Located near the major grouping of high WMDz regions of the extended amygdala module, the ENTm, LA, and TU had high PC values. Interestingly, several of these regions, including the TU, SCs, CEA, LA, and IA, connected strongly with the PAG, pedunculo-pontine nucleus (PPN), and PVT from the midbrain-striatal module, and these regions collectively acted as the major bridge of connectivity between the two modules. The PAG especially acted as a strong hub between the extended amygdala and midbrain-striatal modules (having a high PC value and several connections to regions in the extended amygdala module).

We found that the extended amygdala module and cortico-hippocampo-thalamic module both interacted with the midbrain striatal module exclusively and not with each other. This was unsurprising because the extended amygdala module and cortico-hippocampo-thalamic module were found to have strong anticorrelations with each other. Interestingly, the cortico-hippocampo-thalamic module had numerous brain regions that drove coactivation within its own network, but none of these regions interacted, through positive connectivity, with the other modules. This was evident by the fact that the top 43 WMDz value brain regions of a total of 79 in the cluster had a PC ≤0.10.

Instead, a separate set of regions from the cortico-hippocampo-thalamic module was heavily involved in interactions with the midbrain striatal module, including such regions as the ACB, lateral hypothalamus (LHA), BST, and ventromedial hypothalamic nucleus (VMH), among others.

The midbrain striatal module had several regions that had both high PC values and high WMDz values, such as the medial amygdala (MEA), superior colliculus motor related (SCm), substantia innominata (SI), and MRN, among others. Additionally, both the PAG and PVT had high PC values because of their exclusive connectivity with the extended amygdala module. The PAG especially acted as a strong hub between the extended amygdala and midbrain striatal modules (high PC value connected to regions in the extended amygdala module).

In the extended amygdala module, several brain regions had both high PC values and high WMDz values. These regions included the CEA, IA, and SCs. Additionally, the COAp, PSTN, BLA, and EP had high WMDz values. Connected with the major grouping of high WMDz regions of the extended amygdala module, the ENTm, LA, and TU had high PC values. Interestingly, several of these regions, including the TU, SCs, CEA, LA, and IA, connected strongly with the PAG, PPN, and PVT from the midbrain striatal module, and these regions collectively acted as the major bridge of connectivity between the two modules.

Other regions in the extended amygdala module had high PC values connected to the midbrain striatal module, such as the PIR, claustrum (CLA), GU, retrosplenial area ventral part (RSPv), and olivary pretectal nucleus (OP). These regions were connected to a separate group of regions from the midbrain striatal module that included the ventral agranular insula (AIv),
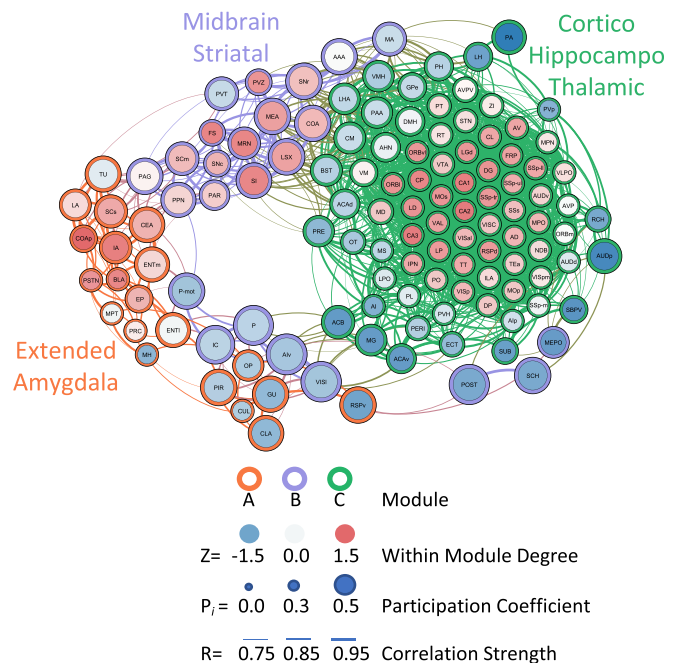
Fig. 6. Functional connectivity of alcohol-dependent mice during abstinence thresholded to 0.75R. Nodes/brain regions of the network are represented by circles. The size of the node represents the PC (smaller = lower PC; larger = higher PC). The internal color of each circle represents the within-module degree Z-score (dark blue = lowest; dark red = highest). The color of the modules that are identified in Fig. 5C are represented by different colored edges of each node circle (red = module A/extended amygdala; blue = module B/midbrain striatal; green = module C/cortico-hippocampo-thalamic). The thickness of the lines represents the strength of the correlation between regions (thin = lower correlation; thick = higher correlation). See figure key for examples of each representative component of the figure.

lateral visual cortex (VISl), inferior colliculus (IC), P, POST, and suprachiasmatic nucleus (SCH). These data, together with the modular structure of the network, indicated that several brain regions contributed to the activity of each module. In the case of the cortico-hippocampo-thalamic module, however, the regions that were involved in intramodule and intermodule connectivity were distinct from each other. Conversely, in the extended amygdala and midbrain striatal modules, several brain regions contributed to both intramodule and intermodule network connectivity.

Discussion

The present study used single-cell whole-brain imaging to determine whether the brain is restructured by alcohol use, alcohol dependence, and abstinence. A history of alcohol drinking resulted in increases in coactivation networks compared with nondrinking controls. Specifically, nondependent subjects exhibited moderate changes in coactivation compared with nondrinkers, whereas abstinence from alcohol dependence resulted in the reorganization of functional coactivation networks compared with both nondependent and naive networks. Brain networks in dependent animals exhibited fewer larger modules of coactivated brain regions, indicating that abstinence is associated with a reduction of modularity. This lower modularity resulted in the emergence of a new network architecture that was different from control conditions, in which the majority of brain regions were coactivated with each other in a cortico-hippocampo-thalamic module but anticorrelated with an extended amygdala module. Using graph theory, we identified candidate hub (i.e., high intra- or intermodule connectivity) regions of the extended amygdala module that may play a critical role in driving neural activity that is associated with alcohol abstinence. These unbiased whole-brain analyses showed that abstinence from alcohol dependence resulted in lower modularity, but whether these changes are a cause or consequence of alcohol dependence is unclear and needs further investigation.

Similar to previous reports (18, 21, 30–32), the present study found an increase in alcohol drinking and signs of affective dysfunction (i.e., digging and irritability-like behavior). Interestingly, we did not observe signs of anhedonia in alcohol-dependent mice as measured by sweet taste preference. Previous studies in C57BL/6J mice also did not find alterations of sweet taste preference in either alcohol-dependent or binge-drinking models (18, 33, 34). However, other strains of mice were reported to exhibit lower sucrose preference after CIE exposure (35), suggesting that the specific mouse strain may be a factor in the development of anhedonia as an aspect of affective dysfunction.

When examining neural activity in each group, we found an increase in coactivation in both alcohol-dependent and nondependent networks compared with the naive network. The increase in coactivation was substantial in the alcohol-dependent network, but the moderate increase in coactivation in the nondependent network suggests that casual drinking may create a pattern of brain activity that is vulnerable to the transition to alcohol dependence. Indeed, in animal models, a prior history of alcohol drinking has been shown to facilitate the transition to alcohol dependence (36).

Using hierarchical clustering, we found a reduction of modularity in the alcohol abstinence functional network (3 modules) compared with the nondependent (9 modules) and naive (10 modules) networks, indicating that alcohol drinking and especially abstinence from alcohol dependence resulted in a less modular brain overall. In humans, a similar decrease in brain modularity has been observed in dementia and after traumatic brain injury (7–12). Decreases in modularity of the brain may be partially responsible for cognitive dysfunction that is seen in humans and animal models of alcohol dependence (37–42). Alcohol is known to be neurotoxic in humans and rodent models.

Heavy usage can lead to dementia through Wernicke–Korsakoff syndrome (43–52), and repeated exposure to drugs can result in changes in synaptic plasticity (53). Thus, our findings may be partially attributable to neurotoxicity and changes in neuroplasticity that are associated with chronic alcohol exposure. Additionally, the use of other drugs of abuse, such as cocaine, has been shown to alter functional connectivity and decrease modularity (24, 54–57).

We next assessed the way in which modular organization of the alcohol abstinence network was related to neurobiological organization of the brain that is proposed in the four major neurobiological theories that may explain excessive alcohol use in dependent subjects: recruitment of the mesolimbic dopamine system (58–60), the recruitment of cortico-striatal loops (61, 62), recruitment of the extended amygdala (63, 64), and the three-stage theory (4, 65, 66) (Fig. 7). We identified three modules that were associated with alcohol abstinence: 1) extended amygdala module, 2) midbrain striatal module, and 3) cortico-hippocampo-thalamic module. Notably, in some cases, brain regions that we would expect to be in one module were actually in another module (e.g., the BST, VTA, and ACB were part of the cortico-hippocampo-thalamic module). The extended amygdala and cortico-hippocampo-thalamic modules had directly opposing activation patterns and included exclusively brain regions from specific anatomical groups. The brain regions in the extended amygdala module (e.g., CEA, IA, BLA, LA PSTN, TU, GU, MH, etc.), which are hypothesized to be involved in negative affect (4), matched directly with the brain regions that are proposed by the extended amygdala and three-stage theories. The cortico-hippocampo-thalamic module had actions that opposed the extended amygdala module and included almost all of the PFC, OFC, HIPP, sensory/somatosensory cortex, THAL, HYPO, VTA, and IPN. Several of these regions (e.g., PFC, OFC, insula, VTA, and ACB) match brain regions that are proposed by the cortico-striatal loops and three-stage theories. The midbrain striatal module contained several regions that are involved in midbrain-striatal dopamine reward signaling (e.g., SNr, SNc, PAG, MRN, lateral septal complex, SI, fundus of striatum, etc.), suggesting that this module fits well with brain regions that are proposed by the mesolimbic dopamine system and three-stage theories. Additionally, the ACB is one of the connector regions between the midbrain-striatal and cortico-hippocampo-thalamic modules. The midbrain striatal module had moderate coactivation with both the extended amygdala and cortico-hippocampo-thalamic modules, suggesting that this group of regions may act to integrate information from the other two modules. Alcohol abstinence results in a major reduction of modular structuring of the brain, similar to other mental disorders (7–12), and the network structure best matches the brain regions and neurobiological organization of a hypothesized three-stage theory (4, 65–67). These data provide evidence that alcohol use and dependence significantly alter the brain, but unclear is whether these alterations of neural coactivation and modularity are a cause or consequence of long-term exposure to alcohol or other factors.

The extended amygdala has been heavily implicated in negative affect during drug withdrawal and protracted abstinence. However, much of the focus of previous studies has been on the CEA and BST (4, 68, 69) and not on connections to other brain regions within this functional module. With regard to alcohol abstinence, the present findings suggest that the extended amygdala as a functional module may need to be redefined to include connections to additional brain areas, such as the PSTN, COAp, IA, EP, and BLA.

Using graph theory, we identified several non-CEA brain regions in the extended amygdala module that may drive alcohol abstinence. The TU was found to have high intermodule connectivity (high PC), primarily through the PAG, suggesting that
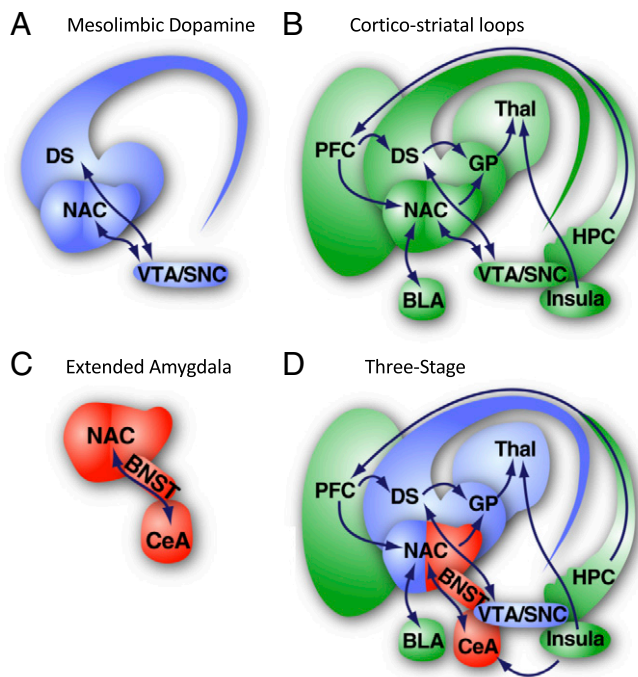
Fig. 7. Theories of brain regions that are involved in the neurobiology of alcohol use disorder. (*A*) Brain regions of the mesolimbic dopamine system. (*B*) Brain regions consisting of cortico-striatal loops. (*C*) Extended amygdalar brain regions. (*D*) Three-stage theory. Images are modified from ref. 4.

the PAG and TU may communicate to drive neural activity during abstinence. The PAG has been shown to be involved in anxiety and hyperalgesia that are associated with alcohol abstinence (69, 70), and chronic alcohol exposure has been found to alter PAG dopamine signaling (71). The PSTN, COAp, EP, and BLA were found to have high intramodule connectivity (high WMDz), suggesting that they may drive activity within the extended amygdala circuit. Both the EP and BLA have been implicated in alcohol abstinence (72–74), but the PSTN and COAp remain understudied. The CEA, SCs, and IA presented both high intramodule and intermodule connectivity (high WMDz and PC), suggesting that these regions may be major drivers of abstinence symptoms and could be ideal targets for further study. The SC is involved in seizure responses during alcohol abstinence (75, 76). The IA, although relatively understudied in alcohol research, contains dopamine D_1 receptors (77), and an increase in D_1 receptor density has been reported in alcohol-preferring rats following repeated alcohol deprivation (78). Many of the understudied brain regions may or may not involve gene transcription, molecular signaling, and circuit pathways that were previously identified to contribute to the transition to excessive drinking and withdrawal (79–81) and may involve novel mechanisms or receptors that are yet to be fully explored (e.g., orphan G protein-coupled receptors) (82), thus warranting further investigations of functional importance.

A known limitation of the present study is the focus on neuronal networks of abstinence (7 d). This time point was chosen because increases in drinking and withdrawal symptoms (see current data) are most robust in the 2BC/CIE mouse model of alcohol dependence after 7 d of abstinence. The network structure that was identified herein would likely be different at other time points (e.g., intoxication, acute withdrawal, and relapse). Follow-up studies will be critical to further understand the structure of the neuronal network of abstinence and its dynamics during different phases of drinking.

The present study demonstrates that alcohol dependence and abstinence significantly decrease modularity and remodel the functional architecture of the brain into three major groups (i.e., a cortico-hippocampo-thalamic module and an extended amygdala module with opposite coactivation patterns and an intermediate midbrain striatal module), thus matching the neurobiological three-stage theory (4, 65, 66) better than any single theory (recruitment of the mesolimbic dopamine system, recruitment of the extended amygdala, and the recruitment of cortico-striatal loops) for the organization of brain regions. Hierarchical clustering and graph theory analyses identified existing and novel hub regions that may drive network dysfunction during alcohol abstinence. Altogether, these results suggest that abstinence from alcohol dependence rather than casual drinking completely remodels the functional architecture of the brain. Future research will be necessary to determine whether changes in coactivation and modularity that are associated with alcohol abstinence are causal features of alcohol dependence or a consequence of excessive drinking and alcohol exposure.

Materials and Methods

Animals. Age-matched male C57BL/6J mice that were bred at The Scripps Research Institute (20 to 30 g) were used for the experiments. The mice were single-housed for the entire duration of the study. The mice were maintained on a 12-h/12-h light/dark cycle with ad libitum access to food and water with 7090 Teklad sani-chips (Envigo) as bedding for the home cages and experimentation. All of the procedures were conducted in strict adherence to the *Guide for the Care and Use of Laboratory Animals* (83) and approved by The Scripps Research Institute Institutional Animal Care and Use Committee.

Behavioral Testing.
Two-bottle choice/CIE vapor. We used the 2BC/CIE paradigm, a well-established mouse model of alcohol dependence (18, 30–32), to induce alcohol dependence, the escalation of alcohol drinking, and behavioral symptoms of abstinence. In the 2BC/CIE paradigm, weeks of voluntary alcohol drinking during limited-access 2BC sessions are alternated with weeks of CIE.

During 2BC weeks, the mice were given access to two bottles that contained water and alcohol (15%, vol/vol), respectively, Monday through Friday for 2 h, starting at the beginning of the dark phase of the circadian cycle. During CIE weeks, the mice were exposed to four cycles of 16-h intoxication/8-h abstinence (Monday through Friday) followed by 72-h abstinence (Friday to Monday). Each 16-h period of alcohol vapor exposure was primed with an intraperitoneal injection of alcohol (1.5 g/kg) to initiate intoxication and pyrazole (an alcohol dehydrogenase inhibitor, 1 mmol/kg) to normalize alcohol clearance rate between individual mice. Average blood alcohol levels were measured periodically at the end of alcohol vapor inhalation periods and averaged (164.6 ± 17.0 mg/dL). Air-exposed mice received injections of pyrazole only.

The mice were first given 2 wk of 2BC (weeks 1 to 2) and were then split into two groups with equivalent baseline intake (nondependent [2BC/Air], *n* = 5; alcohol-dependent [2BC/CIE], *n* = 4). The mice were then subjected to five rounds of alternating weeks of Air/CIE exposure with weeks of 2BC drinking (weeks 3 to 12), followed by an additional sixth week of Air/CIE exposure (week 13). The mice were tested for irritability and digging behaviors 7 and 10 d, respectively, into abstinence from vapor (week 14) and were then exposed to a final seventh week of Air/CIE inhalation (week 15). Alcohol-dependent and nondependent mice were perfused 7 d after the last vapor/air exposure, with no intervening behavioral testing or voluntary drinking, at the same time of day as 2BC sessions would occur in previous weeks (week 16). The mice were removed directly from their home cages immediately before tissue collection. Brains from age-matched single-housed alcohol-naive mice (*n* = 5) were also collected at the same time.
Irritability-like behavior. Irritability is a central feature of alcohol dependence in humans, together with greater aggression and frustration (84–88). Irritability-like behavior was assessed using the bottle brush test (BBT), conducted as described by Riittinen et al. (89). The BBT measures defensive and aggressive responses to an "attack" by a mechanical stimulus (i.e., a moving bottle brush) (90). The BBT has recently been used in alcohol-dependent rats and mice to identify increases in irritability-like behavior during alcohol abstinence (19–21). The methods were similar to Sidhu et al. (21). Testing was conducted under red light. The mouse was "attacked" by moving a bottle brush (14-cm length × 5-cm width cylindrical brush, 33-cm total length with handle) toward it. The attacks were made in the home

Kimbrough et al.

www.manaraa.com

NEUROSCIENCE

cage with the lid and food tray removed. Each test consisted of 10 trials with 10-s intertrial intervals. Briefly, the mouse started each trial at the opposite end of the cage and was then "attacked" by the brush. Each attack consisted of five stages: 1) the brush rotating toward the mouse from the opposite end of the cage, 2) the brush rotating against the whiskers of the mouse, 3) the brush rotating backward toward the starting position in the opposite end of the cage, 4) the brush rotating at the starting position, and 5) the brush at the starting position not rotating. Each stage lasted 1.5 s, with the exception of stage 5 that was prolonged, if necessary, until the mouse returned to its end of the cage or 5 s elapsed. Responses to the attacks were observed by an observer who was blind to treatment group. The following behavioral responses were scored: smelling the brush, exploring the brush, biting the brush, boxing the brush, following the brush, tail rattling, escaping from the brush, digging, jumping, climbing/rearing, defecation, vocalization, and grooming. The total number of occurrences of each behavior across all 10 trials was recorded and summed to calculate a total irritability-like behavior score.

Digging and marble burying. Digging and marble burying were measured as described by Deacon (91) and Sidhu et al. (21). Testing was conducted under dim lighting (20 lx). The mouse was placed in a new, clean cage with a bedding thickness of 5 cm and no lid and allowed to freely dig for 3 min. The number of digging bouts and total digging duration were recorded (phase 1). The mouse was then removed from the cage. The bedding was flattened, and 12 marbles were arranged in a 4×3 array on top of the bedding. The mouse was reintroduced to the cage and allowed to bury the marbles for 30 min with a lid that covered the cage. The number of marbles that were buried (covered two-thirds or more by bedding) was counted at the end of the test (phase 2) by an observer who was blind to treatment group.

Saccharin preference testing. A separate cohort of alcohol-dependent ($n = 8$), nondependent ($n = 10$), and naive ($n = 8$) mice was tested for saccharin intake using a 2BC procedure with saccharin (1% wt/vol) and water. Prior to testing, the mice were run under the same 2BC/CIE or 2BC/Air protocol as described above for 2BC/CIE vapor. Naive mice were presented with two bottles of water for the same duration as alcohol-dependent and nondependent mice that were presented with two bottles with alcohol and water for 2BC sessions. Saccharin 2BC testing started 12 d after the last CIE exposure (for alcohol-dependent mice) and lasted for seven consecutive days. The average intake (expressed as milligrams per kilogram per 24 h) was recorded across all 7 d of testing for analysis.

Tissue Collection. For alcohol-dependent and nondependent mice, brains were collected 7 d after the last vapor/air exposure, with no intervening behavioral testing or voluntary drinking, at the same time of day as 2BC sessions would normally occur in previous weeks. The mice were removed directly from their home cages immediately prior to tissue collection. Brains from age-matched, single-housed, alcohol-naive mice ($n = 5$) were also collected at the same time. The mice were deeply anesthetized and perfused with 15 mL of phosphate-buffered saline (PBS) followed by 50 mL of 4% paraformaldehyde. The brains were postfixed in paraformaldehyde overnight. The next day, brains were washed for 30 min three times with PBS and transferred to a PBS/0.1% azide solution at 4 °C for 2 to 3 d before processing via iDISCO+.

iDISCO+. To evaluate neuronal recruitment during alcohol abstinence, we used single-cell whole-brain imaging using iDISCO+ with immunohistochemistry to detect immediate early gene c-*fos* expression as a proxy for neuronal activation (14, 17). c-*fos* was chosen over other immediate early genes because its low baseline levels are optimal for detecting increases in neuronal activity and based on previous success using Fos with the iDISCO+ technique by Renier et al. (14, 17). The iDISCO+ procedure was performed as reported by Renier et al. (14, 17).

Immunostaining. Fixed samples were washed in 20% methanol (in double-distilled H_2O) for 1 h, 40% methanol for 1 h, 60% methanol for 1 h, 80% methanol for 1 h, and 100% methanol for 1 h twice. The samples were then precleared with overnight incubation in 33% methanol/66% dichloromethane (DCM; 270997-12 X100ML; Sigma). The next day, the samples were bleached with 5% H_2O_2 (1 volume of 30% H_2O_2 for 5 volumes of methanol, ice cold) at 4 °C overnight. After bleaching, the samples were slowly reequilibrated at room temperature and rehydrated in 80% methanol in double-distilled H_2O for 1 h, 60% methanol for 1 h, 40% methanol for 1 h, 20% methanol for 1 h, PBS for 1 h, and PBS/0.2% TritonX-100 for 1 h twice. The samples were then incubated in PBS/0.2% TritonX-100/20% dimethyl sulfoxide (DMSO)/0.3 M glycine at 37 °C for 2 d and then blocked in PBS/0.2% TritonX-100/10% DMSO/6% donkey serum at 37 °C for 2 d. The samples were then incubated in rabbit anti-c-*fos* (1:500, sc-52; Santa Cruz Bio-

technology) in PBS–0.2% Tween with 10 μg/mL heparin (PTwH)/5% DMSO/3% donkey serum at 37 °C for 7 d. The samples were then washed in PTwH for 24 h (five changes of the PTwH solution over that time) and incubated in donkey anti-rabbit Alexa647 (1:500, A31573; Invitrogen) in PTwH/3% donkey serum at 37 °C for 7 d. The samples were finally washed in PTwH for 1 d before clearing and imaging.

Sample clearing. Immunolabeled brains were cleared using the procedure of Renier et al. (17). The samples were dehydrated in 20% methanol (in double-distilled H_2O) for 1 h, 40% methanol for 1 h, 60% methanol for 1 h, 80% methanol for 1 h, 100% methanol for 1 h, and 100% methanol again overnight. The next day, the samples were incubated for 3 h in 33% methanol/66% DCM until they sank to the bottom of the incubation tube. The methanol was then washed for 20 min twice in 100% DCM. Finally, the samples were incubated in DiBenzyl Ether (DBE; 108014-1KG; Sigma) until clear and then stored in DBE at room temperature until imaged.

Image acquisition. Left hemispheres of cleared samples were imaged in the sagittal orientation (right lateral side up) on a light-sheet microscope (Ultramicroscope II; LaVision Biotec) equipped with a scientific complementary metal–oxide–semiconductor camera (Andor Neo), 2×/0.5 objective lens (MVPLAPO 2×), and 6-mm working distance dipping cap. Imspector microscope controller v144 software was used. The microscope was equipped with an NKT Photonics SuperK EXTREME EXW-12 white light laser with three fixed light-sheet-generating lenses on each side. Scans were made at 0.8× magnification (1.6× effective magnification) with a light-sheet numerical aperture of 0.148. Excitation filters of 480/30, 560/40, and 630/30 were used. Emission filters of 525/50, 595/40, and 680/30 were used. The samples were scanned with a step size of 3 μm using dynamic horizontal scanning from one side (the right) for the 560- and 630-nm channels (20 acquisitions per plane with 240-ms exposure, combined into one image using the horizontal adaptive algorithm) and without horizontal scanning for the 480-nm channel using two-sided illumination (100-ms exposure for each side, combined into one image using the blending algorithm). To accelerate acquisition, both channels where acquired in two separate scans. To account for micromovements of the samples that may occur between scans, 3D image affine registration was performed to align both channels using ClearMap (17).

Data Analysis. Behavioral data were analyzed, and Pearson correlations were calculated using Statistica software (Tibco). Hierarchical clustering was performed using R Studio software. Drinking data are presented as average weekly intake for 2BC sessions. The drinking data were analyzed using repeated-measures ANOVA of the average baseline intake and the last 2 wk of drinking. Post hoc analysis was performed using the SNK test. Nondependent mice and naive mice did not show significant differences in any measure of irritability-like behavior or digging behavior and thus were combined into a single control group for analyses of these data. Irritability-like behavior and digging behavior were analyzed using *t* tests. Values of $P < 0.05$ were considered significant for alcohol-dependent vs. control mice. Digging behavior (number of bouts, duration of bouts, and number of marbles buried) was combined into a single digging value by calculating the Z-score for each individual behavior for all animals across all treatments and then calculating the average Z-score across all three behaviors for each animal.

Identification of Activated Brain Regions. Images that were acquired from the light-sheet microscope were analyzed from the end of the olfactory bulbs (the olfactory bulbs were not included in the analysis) to the beginning of the hindbrain and cerebellum. Counts of Fos-positive nuclei from each sample were identified for each brain region using ClearMap (17). ClearMap uses autofluorescence that is acquired in the 488 channel to align the brain to the Allen Mouse Brain Atlas (92) and then registers Fos counts to regions that are annotated by the atlas. The data were normalized to a $\log_{10}$ value to reduce variability and bring brain regions with high numbers (e.g., thousands) and lower numbers (e.g., tens to hundreds) of Fos counts to a similar scale.

Identification of Coactivation within Individual Networks. Separate interregional Pearson correlations were then calculated across animals for the alcohol-dependent, nondependent, and naive groups to compare the $\log_{10}$ Fos data from each brain region to each of the other brain regions. For all of the functional coactivation network analyses, the nondependent and naive groups were analyzed separately to maintain a relatively equal *n* ($n = 4$ for alcohol-dependent, $n = 5$ for nondependent, and $n = 5$ for naive) for the correlation calculations. Instead of using an alphabetical arrangement of each anatomical group from the Allen Mouse Brain Atlas (92), we split

Kimbrough et al.

www.manaraa.com

the alcohol-dependent interregional Fos correlations into individual anatomical groups (i.e., cortical plate, cortical subplate, striatum, pallidum, thalamus, hypothalamus, and midbrain plus hindbrain). We then calculated the complete Euclidean distance and performed hierarchical clustering of each individual Allen Mouse Brain Atlas group separately. We then rearranged the order of the brain regions for each group based on hierarchical clustering. Using this order for each anatomical Allen Mouse Brain Atlas group, we then merged the groups back together, resulting in an "ordered Allen Mouse Brain Atlas list," which was then applied to arrange the heat maps of correlations for all treatments (Fig. 3 A–C). This arrangement did not alter the values in any way and was used solely for visualization purposes.

Analysis of Amygdala Cluster vs. Other Major Brain Clusters. For each treatment condition, average R values were calculated for correlations between each individual brain region of the amygdala cluster and all brain regions from each of the other clusters that were examined (e.g., average R for CEA to cortical regions). An average and SEM were then calculated across the average R values for all of the amygdala brain regions for each given comparison. A one-way ANOVA was then performed to examine the effect of treatment condition on the average R value for each amygdala vs. other cluster comparison (e.g., average R for amygdala to cortical regions).

Hierarchical Clustering. Previous rat and mouse studies that examined functional connectivity used five to eight animals (23, 24). The number of samples that are examined in functional connectivity studies is the number of potential connections (i.e., 123 total brain regions all connecting with each other). Furthermore, hierarchical clustering organizes brain regions into modules by grouping regions that show a similar coactivation profile across all other brain regions. Thus, more total connections minimize the effect that an inaccurate brain region-to-brain region connection has on network organization and overall network structure.

Hierarchical clustering of distance matrices that were associated with the coactivation network of each condition was used to identify modular structuring of the brain (93–96). Interregional Fos correlations were used to calculate complete Euclidean distances between each pair of brain regions in each group of mice. The distance matrices were then hierarchically clustered by both row and column using the complete method to identify modules of coactivation within each treatment group. The hierarchical cluster dendrograms were trimmed at half the height of each given tree to split the dendrogram into specific modules. The result of tree cutting was consistent across multiple tree-cutting thresholds (Fig. 5D).

Graph Theory Identification of Functional Networks. We used a graph theory-based approach to identify the functional neural network of abstinence symptoms that are seen in alcohol dependence. Graph theory is a branch of mathematics that is used to analyze complex networks, such as social, financial, protein, and neural networks (23, 97–108). Using graph theory, functional networks can be delineated, and key brain regions of the network can be identified (23, 100, 109, 110).

Previous studies of regional connectivity profiles in Fos coactivation networks focused on global measures of connectivity (e.g., degree) (26, 79). However, in correlation-based networks, these measures can be strongly influenced by the size of the subnetwork (module) in which a node participates (111). For the graph theory analyses, we were interested in regional properties and not module size per se. Thus, module structure needs to be considered when examining the role that each region plays in the network. To accomplish this, we utilized two widely used centrality metrics that were designed for application to modular systems. The WMDz indexes the relative importance of a region within its own module

(e.g., intramodule connectivity), and the PC indexes the extent to which a region connects diversely to multiple modules (e.g., intermodule connectivity) (29).

We first took the Pearson correlation values that were calculated for the brain regions from alcohol-dependent mice. Prior to plotting and calculating regional connectivity metrics, the network was thresholded to remove any edges that were weaker than $R = 0.75$. As such, visualization and graph theory analyses were performed using only edges with positive weights. Regional connectivity metrics (PC and WMDz) were calculated as originally defined by Guimerà and Nunes Amaral (29), modified for application to networks with weighted edges. PC and WMDz were calculated using a customized version of the bctpy Python package (https://github.com/aestrivex/bctpy), which is derived from the MATLAB implementation of Brain Connectivity Toolbox (109).

For WMDz, let k_i (within-module degree) be the summed weight of all edges between region i and other regions in module s_i. Then, $\bar{k}_{s_i}$ is the average within-module degree of all regions in module s_i, and $\sigma_{k_{s_i}}$ is the SD of those values. The Z-scored version of within-module degree (WMDz) is then defined as

$$WMDz = \frac{k_i - \bar{k}_{s_i}}{\sigma_{k_{s_i}}}.$$

This provides a measure of the extent to which each region is connected to other regions in the same module.

For PC, let k_{is} (between-module degree) be the summed weight of all edges between region i and regions in module s, and let k_i (total degree) be the summed weight of all edges between region i and all other regions in the network. The PC of each region is then defined as

$$P_i = 1 - \sum_{s=1}^{N_M} \left(\frac{k_{is}}{k_i} \right)^2.$$

This provides a measure of the extent to which the connections of a region are distributed mostly within its own module (PC approaching 0) or distributed evenly among all modules (PC approaching 1).

A high PC was considered ≥0.30, and a high WMDz was considered ≥0.70. Previous studies have used ranges of ≥0.30 to 0.80 for high PC and ≥1.5 to 2.5 for high WMDz (29, 108). Because of differences in the sizes/types of networks that were examined and the methods that were used (e.g., Fos vs. functional magnetic resonance imaging), our WMDz values were considerably lower overall (ranging from −1.5 to 1.5). Therefore, we adjusted the range for high WMDz accordingly. This resulted in 7/20 regions for the extended amygdala module, 9/24 for the midbrain-striatal module, and 25/79 for the cortico-hippocampo-thalamic module that were considered to have high WMDz.

Network visualization was performed using a combination of Gephi 0.9.2 software (112) and Adobe Illustrator software. Nodes were positioned using the Force Atlas 2 algorithm (113).

Data Availability. Data will be made available upon request.

1. SAMHSA, Alcohol use disorder in the past year, by age group and state: Percentages, annual averages based on 2014 and 2015 NSDUHs. https://www.samhsa.gov, https://www.samhsa.gov/data/population-data-nsduh/reports. Accessed 31 December 2019.
2. G. Addolorato, A. Mirijello, L. Leggio, A. Ferrulli, R. Landolfi, Management of alcohol dependence in patients with liver disease. *CNS Drugs* **27**, 287–299 (2013).
3. H. R. Noori, R. Spanagel, A. C. Hansson, Neurocircuitry for modeling drug effects. *Addict. Biol.* **17**, 827–864 (2012).
4. G. F. Koob, N. D. Volkow, Neurobiology of addiction: A neurocircuitry analysis. *Lancet Psychiatry* **3**, 760–773 (2016).
5. M. Heilig, W. H. Sommer, R. Spanagel, The need for treatment responsive translational biomarkers in alcoholism research. *Curr. Top. Behav. Neurosci.* **28**, 151–171 (2016).
6. D. Belin, A. Belin-Rauscent, B. J. Everitt, J. W. Dalley, In search of predictive endophenotypes in addiction: Insights from preclinical research. *Genes Brain Behav.* **15**, 74–88 (2016).
7. C. L. Gallen et al., Modular brain network organization predicts response to cognitive training in older adults. *PLoS One* **11**, e0169015 (2016).
8. M. A. Bertolero, B. T. T. Yeo, D. S. Bassett, M. D'Esposito, A mechanistic model of connector hubs, modularity and cognition. *Nat. Hum. Behav.* **2**, 765–777 (2018).
9. W. de Haan et al., Disrupted modular brain dynamics reflect cognitive dysfunction in Alzheimer's disease. *Neuroimage* **59**, 3085–3093 (2012).
10. M. R. Brier et al., Functional connectivity and graph theory in preclinical Alzheimer's disease. *Neurobiol. Aging* **35**, 757–768 (2014).
11. O. Sporns, R. F. Betzel, Modular brain networks. *Annu. Rev. Psychol.* **67**, 613–640 (2016).
12. K. L. Arnemann et al., Functional brain network modularity predicts response to cognitive training after brain injury. *Neurology* **84**, 1568–1574 (2015).
13. K. Chung, K. Deisseroth, CLARITY for mapping the nervous system. *Nat. Methods* **10**, 508–513 (2013).

Kimbrough et al.

14. N. Renier et al., iDISCO: A simple, rapid method to immunolabel large tissue samples for volume imaging. *Cell* **159**, 896–910 (2014).

15. A. Azaripour et al., A survey of clearing techniques for 3D imaging of tissues with special reference to connective tissue. *Prog. Histochem. Cytochem.* **51**, 9–23 (2016).

16. J. Seo, M. Choe, S. Y. Kim, Clearing and labeling techniques for large-scale biological tissues. *Mol. Cells* **39**, 439–446 (2016).

17. N. Renier et al., Mapping of brain activity by automated volume analysis of immediate early genes. *Cell* **165**, 1789–1802 (2016).

18. H. C. Becker, M. F. Lopez, Increased ethanol drinking after repeated chronic ethanol exposure and withdrawal experience in C57BL/6 mice. *Alcohol. Clin. Exp. Res.* **28**, 1829–1838 (2004).

19. S. S. Somkuwar et al., Abstinence from prolonged ethanol exposure affects plasma corticosterone, glucocorticoid receptor signaling and stress-related behaviors. *Psychoneuroendocrinology* **84**, 17–31 (2017).

20. A. Kimbrough et al., CRF₁ receptor-dependent increases in irritability-like behavior during abstinence from chronic intermittent ethanol vapor exposure. *Alcohol. Clin. Exp. Res.* **41**, 1886–1895 (2017).

21. H. Sidhu, M. Kreifeldt, C. Contet, Affective disturbances during withdrawal from chronic intermittent ethanol inhalation in C57BL/6J and DBA/2J male mice. *Alcohol. Clin. Exp. Res.* **42**, 1281–1290 (2018).

22. S. Scheggi, De Montis, Gambarana C (2018) Making sense of rodent models of anhedonia. *Int. J. Neuropsychopharmacol.* **21**, 1049–1065.

23. A. L. Wheeler et al., Identification of a functional connectome for long-term fear memory in mice. *PLoS Comput. Biol.* **9**, e1002853 (2013).

24. C. A. Orsini, L. M. Colon-Perez, S. C. Heshmati, B. Setlow, M. Febo, Functional connectivity of chronic cocaine use reveals progressive neuroadaptations in neocortical, striatal, and limbic networks. *eNeuro* **5**, ENEURO.0081-18.2018 (2018).

25. F. Giove, T. Gili, V. Iacovella, E. Macaluso, B. Maraviglia, Images-based suppression of unwanted global signals in resting-state functional connectivity studies. *Magn. Reson. Imaging* **27**, 1058–1064 (2009).

26. G. Chen, G. Chen, C. Xie, S. J. Li, Negative functional connectivity and its dependence on the shortest path length of positive network in the resting-state human brain. *Brain Connect.* **1**, 195–206 (2011).

27. K. Murphy, R. M. Birn, D. A. Handwerker, T. B. Jones, P. A. Bandettini, The impact of global signal regression on resting state correlations: Are anti-correlated networks introduced? *Neuroimage* **44**, 893–905 (2009).

28. D. Meunier, S. Achard, A. Morcom, E. Bullmore, Age-related changes in modular organization of human brain functional networks. *Neuroimage* **44**, 715–723 (2009).

29. R. Guimerà, L. A. Nunes Amaral, Functional cartography of complex metabolic networks. *Nature* **433**, 895–900 (2005).

30. C. Contet et al., Identification of genes regulated in the mouse extended amygdala by excessive ethanol drinking associated with dependence. *Addict. Biol.* **16**, 615–619 (2011).

31. M. Kreifeldt, D. Le, S. N. Treistman, G. F. Koob, C. Contet, BK channel β1 and β4 auxiliary subunits exert opposite influences on escalated ethanol drinking in dependent mice. *Front. Integr. Nuerosci.* **7**, 105 (2013).

32. G. Gorini, A. J. Roberts, R. D. Mayfield, Neurobiological signatures of alcohol dependence revealed by protein profiling. *PLoS One* **8**, e82656 (2013).

33. J. J. Olney, S. A. Marshall, T. E. Thiele, Assessment of depression-like behavior and anhedonia after repeated cycles of binge-like ethanol drinking in male C57BL/6J mice. *Pharmacol. Biochem. Behav.* **168**, 1–7 (2018).

34. K. M. Lee, M. Coehlo, H. A. McGregor, R. S. Waltermire, K. K. Szumlinski, Binge alcohol drinking elicits persistent negative affect in mice. *Behav. Brain Res.* **291**, 385–398 (2015).

35. P. Metten et al., An alcohol withdrawal test battery measuring multiple behavioral symptoms in mice. *Alcohol* **68**, 19–35 (2018).

36. A. Kimbrough, S. Kim, M. Cole, M. Brennan, O. George, Intermittent access to ethanol drinking facilitates the transition to excessive drinking after chronic intermittent ethanol vapor exposure. *Alcohol. Clin. Exp. Res.* **41**, 1502–1509 (2017).

37. H. M. Golub et al., Chronic alcohol exposure is associated with decreased neurogenesis, aberrant integration of newborn neurons, and cognitive dysfunction in female mice. *Alcohol. Clin. Exp. Res.* **39**, 1967–1977 (2015).

38. O. A. Parsons, S. J. Nixon, Neurobehavioral sequelae of alcoholism. *Neurol. Clin.* **11**, 205–218 (1993).

39. E. V. Sullivan, M. J. Rosenbloom, A. Pfefferbaum, Pattern of motor and cognitive deficits in detoxified alcoholic men. *Alcohol. Clin. Exp. Res.* **24**, 611–621 (2000).

40. T. H. McKim, D. J. Bauer, C. A. Boettiger, Addiction history associates with the propensity to form habits. *J. Cogn. Neurosci.* **28**, 1024–1038 (2016).

41. A. P. Le Berre, R. Fama, E. V. Sullivan, Executive functions, memory, and social cognitive deficits and recovery in chronic alcoholism: A critical review to inform future research. *Alcohol. Clin. Exp. Res.* **41**, 1432–1443 (2017).

42. F. T. Crews, C. A. Boettiger, Impulsivity, frontal lobes and risk for addiction. *Pharmacol. Biochem. Behav.* **93**, 237–247 (2009).

43. N. M. Zahr, A. Pfefferbaum, Alcohol's effects on the brain: Neuroimaging results in humans and animal models. *Alcohol Res.* **38**, 183–206 (2017).

44. S. De Santis et al., Microstructural white matter alterations in men with alcohol use disorder and rats with excessive alcohol consumption during early abstinence. *JAMA Psychiatry* **76**, 749–758 (2019).

45. J. G. Hashimoto, K. M. Wiren, C. J. Wilhelm, A neurotoxic alcohol exposure paradigm does not induce hepatic encephalopathy. *Neurotoxicol. Teratol.* **56**, 35–40 (2016).

46. C. D. Mandyam, The interplay between the Hippocampus and amygdala in regulating aberrant hippocampal neurogenesis during protracted abstinence from alcohol dependence. *Front. Psychiatry* **4**, 61 (2013).

47. N. M. Zahr et al., In vivo evidence for alcohol-induced neurochemical changes in rat brain without protracted withdrawal, pronounced thiamine deficiency, or severe liver damage. *Neuropsychopharmacology* **34**, 1427–1442 (2009).

48. A. Pfefferbaum et al., Ventricular expansion in wild-type Wistar rats after alcohol exposure by vapor chamber. *Alcohol. Clin. Exp. Res.* **32**, 1459–1467 (2008).

49. W. M. Vargas, L. Bengston, N. W. Gilpin, B. W. Whitcomb, H. N. Richardson, Alcohol binge drinking during adolescence or dependence during adulthood reduces prefrontal myelin in male rats. *J. Neurosci.* **34**, 14777–14782 (2014).

50. H. N. Richardson et al., Permanent impairment of birth and survival of cortical and hippocampal proliferating cells following excessive drinking during alcohol dependence. *Neurobiol. Dis.* **36**, 1–10 (2009).

51. E. Isenberg-Grzeda, H. E. Kutner, S. E. Nicolson, Wernicke-Korsakoff-syndrome: Under-recognized and under-treated. *Psychosomatics* **53**, 507–516 (2012).

52. E. Day, P. W. Bentham, R. Callaghan, T. Kuruvilla, S. George, Thiamine for prevention and treatment of Wernicke-Korsakoff Syndrome in people who abuse alcohol. *Cochrane Database Syst. Rev.*, CD004033 (2013).

53. F. Kasanetz et al., Transition to addiction is associated with a persistent impairment in synaptic plasticity. *Science* **328**, 1709–1712 (2010).

54. D. Tomasi et al., Disrupted functional connectivity with dopaminergic midbrain in cocaine abusers. *PLoS One* **5**, e10815 (2010).

55. A. B. Konova, S. J. Moeller, D. Tomasi, R. Z. Goldstein, Effects of chronic and acute stimulants on brain functional connectivity hubs. *Brain Res.* **1628**, 147–156 (2015).

56. A. B. Konova, S. J. Moeller, D. Tomasi, N. D. Volkow, R. Z. Goldstein, Effects of methylphenidate on resting-state functional connectivity of the mesocorticolimbic dopamine pathways in cocaine addiction. *JAMA Psychiatry* **70**, 857–868 (2013).

57. X. Liang et al., Interactions between the salience and default-mode networks are disrupted in cocaine addiction. *J. Neurosci.* **35**, 8081–8090 (2015).

58. T. E. Robinson, K. C. Berridge, Review. The incentive sensitization theory of addiction: Some current issues. *Philos. Trans. R. Soc. Lond. B Biol. Sci.* **363**, 3137–3146 (2008).

59. K. C. Berridge, T. E. Robinson, Liking, wanting, and the incentive-sensitization theory of addiction. *Am. Psychol.* **71**, 670–679 (2016).

60. T. E. Robinson, K. C. Berridge, The neural basis of drug craving: An incentive-sensitization theory of addiction. *Brain Res. Brain Res. Rev.* **18**, 247–291 (1993).

61. B. J. Everitt, T. W. Robbins, Neural systems of reinforcement for drug addiction: From actions to habits to compulsion. *Nat. Neurosci.* **8**, 1481–1489 (2005).

62. B. J. Everitt, Neural and psychological mechanisms underlying compulsive drug seeking habits and drug memories–Indications for novel treatments of addiction. *Eur. J. Neurosci.* **40**, 2163–2182 (2014).

63. G. F. Koob, Hedonic homeostatic dysregulation as a driver of drug-seeking behavior. *Drug Discov. Today Dis. Models* **5**, 207–215 (2008).

64. O. George, M. Le Moal, G. F. Koob, Allostasis and addiction: Role of the dopamine and corticotropin-releasing factor systems. *Physiol. Behav.* **106**, 58–64 (2012).

65. G. F. Koob, M. Le Moal, Drug abuse: Hedonic homeostatic dysregulation. *Science* **278**, 52–58 (1997).

66. G. F. Koob, N. D. Volkow, Neurocircuitry of addiction. *Neuropsychopharmacology* **35**, 217–238 (2010).

67. L. E. Kwako, R. Momenan, R. Z. Litten, G. F. Koob, D. Goldman, Addictions neuroclinical assessment: A neuroscience-based framework for addictive disorders. *Biol. Psychiatry* **80**, 179–189 (2016).

68. K. E. Pleil et al., Effects of chronic ethanol exposure on neuronal function in the prefrontal cortex and extended amygdala. *Neuropharmacology* **99**, 735–749 (2015).

69. E. M. Avegno et al., Central amygdala circuits mediate hyperalgesia in alcohol-dependent rats. *J. Neurosci.* **38**, 7761–7773 (2018).

70. V. T. Bonassoli, E. B. Contardi, H. Milani, R. M. de Oliveira, Effects of nitric oxide synthase inhibition in the dorsolateral periaqueductal gray matter on ethanol withdrawal-induced anxiety-like behavior in rats. *Psychopharmacology (Berl.)* **228**, 487–498 (2013).

71. C. Li, N. M. McCall, A. J. Lopez, T. L. Kash, Alcohol effects on synaptic transmission in periaqueductal gray dopamine neurons. *Alcohol* **47**, 279–287 (2013).

72. B. Ruggeri et al., Neuropeptide S receptor gene expression in alcohol withdrawal and protracted abstinence in postdependent rats. *Alcohol. Clin. Exp. Res.* **34**, 90–97 (2010).

73. M. Morales, M. M. McGinnis, S. L. Robinson, A. M. Chappell, B. A. McCool, Chronic intermittent ethanol exposure modulation of glutamatergic neurotransmission in rat lateral/basolateral amygdala is duration-, input-, and sex-dependent. *Neuroscience* **371**, 277–287 (2018).

74. M. R. Diaz, D. T. Christian, N. J. Anderson, B. A. McCool, Chronic ethanol and withdrawal differentially modulate lateral/basolateral amygdala paracapsular and local GABAergic synapses. *J. Pharmacol. Exp. Ther.* **337**, 162–170 (2011).

75. J. Peris, M. Coleman-Hardee, J. Burry, M. Pecins-Thompson, Selective changes in GABAergic transmission in substantia nigra and superior colliculus caused by ethanol and ethanol withdrawal. *Alcohol. Clin. Exp. Res.* **16**, 311–319 (1992).

76. L. Yang, C. Long, C. L. Faingold, Neurons in the deep layers of superior colliculus are a requisite component of the neuronal network for seizures during ethanol withdrawal. *Brain Res.* **920**, 134–141 (2001).

77. K. Fuxe et al., The dopamine D1 receptor-rich main and paracapsular intercalated nerve cell groups of the rat amygdala: Relationship to the dopamine innervation. *Neuroscience* **119**, 733–746 (2003).

78. Y. Sari, R. L. Bell, F. C. Zhou, Effects of chronic alcohol and repeated deprivations on dopamine D1 and D2 receptor levels in the extended amygdala of inbred alcohol-preferring rats. *Alcohol. Clin. Exp. Res.* **30**, 46–56 (2006).

79. J. Le Merrer et al., Protracted abstinence from distinct drugs of abuse shows regulation of a common gene network. *Addict. Biol.* **17**, 1–12 (2012).

80. L. Hwa, J. Besheer, T. Kash, Glutamate plasticity woven through the progression to alcohol use disorder: A multi-circuit perspective. *F1000 Res.* **6**, 298 (2017).

81. D. Ron, S. Barak, Molecular mechanisms underlying alcohol-drinking behaviours. *Nat. Rev. Neurosci.* **17**, 576–591 (2016).

82. A. T. Ehrlich *et al.*, Expression map of 78 brain-expressed mouse orphan GPCRs provides a translational resource for neuropsychiatric research. *Commun. Biol.* **1**, 102 (2018).

83. National Research Council, Guide for the Care and Use of Laboratory Animals (National Academies Press, Washington, DC, ed. 8, 2011).

84. K. A. Miczek, J. F. DeBold, L. S. Hwa, E. L. Newman, R. M. de Almeida, Alcohol and violence: Neuropeptidergic modulation of monoamine systems. *Ann. N. Y. Acad. Sci.* **1349**, 96–118 (2015).

85. J. M. Cardoso, A. Barbosa, F. Ismail, S. Pombo, NETER alcoholic typology (NAT). *Alcohol Alcohol.* **41**, 133–139 (2006).

86. J. L. Winward, N. M. Bekman, K. L. Hanson, C. W. Lejuez, S. A. Brown, Changes in emotional reactivity and distress tolerance among heavy drinking adolescents during sustained abstinence. *Alcohol. Clin. Exp. Res.* **38**, 1761–1769 (2014).

87. M. Y. Baars, M. J. Müller, B. Gallhofer, P. Netter, Relapse (number of detoxifications) in abstinent male alcohol-dependent patients as related to personality traits and types of tolerance to frustration. *Neuropsychobiology* **67**, 241–248 (2013).

88. A. Lubman, C. Emrick, W. F. Mosimann, R. Freedman, Altered mood and norepinephrine metabolism following withdrawal from alcohol. *Drug Alcohol Depend.* **12**, 3–13 (1983).

89. M. L. Riittinen *et al.*, Impoverished rearing conditions increase stress-induced irritability in mice. *Dev. Psychobiol.* **19**, 105–111 (1986).

90. K. Lagerspetz, R. Portin, Simulation of cues eliciting aggressive responses in mice at two age levels. *J. Genet. Psychol.* **113**, 53–63 (1968).

91. R. M. Deacon, Digging and marble burying in mice: Simple methods for in vivo identification of biological impacts. *Nat. Protoc.* **1**, 122–124 (2006).

92. Anonymous, *Allen Mouse Brain Atlas* (Allen Institute for Brain Science, 2004).

93. J. W. Lin *et al.*, Signatures of malaria-associated pathology revealed by high-resolution whole-blood transcriptomics in a rodent model of malaria. *Sci. Rep.* **7**, 41722 (2017).

94. J. Wang, M. Li, J. Chen, Y. Pan, A fast hierarchical clustering algorithm for functional modules discovery in protein interaction networks. *IEEE/ACM Trans. Comput. Biol. Bioinformatics* **8**, 607–620 (2011).

95. E. I. Kanonidis, M. M. Roy, R. F. Deighton, T. Le Bihan, Protein Co-expression analysis as a strategy to complement a standard quantitative proteomics approach: Case of a glioblastoma multiforme study. *PLoS One* **11**, e0161828 (2016).

96. S. Ray, S. M. M. Hossain, L. Khatun, A. Mukhopadhyay, A comprehensive analysis on preservation patterns of gene co-expression networks during Alzheimer's disease progression. *BMC Bioinformatics* **18**, 579 (2017).

97. H. Jeong, S. P. Mason, A. L. Barabási, Z. N. Oltvai, Lethality and centrality in protein networks. *Nature* **411**, 41–42 (2001).

98. A. L. Barabási, Scale-free networks: A decade and beyond. *Science* **325**, 412–413 (2009).

99. M. Babu *et al.*, Interaction landscape of membrane-protein complexes in Saccharomyces cerevisiae. *Nature* **489**, 585–589 (2012).

100. G. Vetere *et al.*, Chemogenetic interrogation of a brain-wide fear memory network in mice. *Neuron* **94**, 363–374.e4 (2017).

101. T. A. Jarrell *et al.*, The connectome of a decision-making neural network. *Science* **337**, 437–444 (2012).

102. S. W. Oh *et al.*, A mesoscale connectome of the mouse brain. *Nature* **508**, 207–214 (2014).

103. L. R. Varshney, B. L. Chen, E. Paniagua, D. H. Hall, D. B. Chklovskii, Structural properties of the Caenorhabditis elegans neuronal network. *PLoS Comput. Biol.* **7**, e1001066 (2011).

104. N. T. Markov *et al.*, A weighted and directed interareal connectivity matrix for macaque cerebral cortex. *Cereb. Cortex* **24**, 17–36 (2014).

105. A. S. Chiang *et al.*, Three-dimensional reconstruction of brain-wide wiring networks in Drosophila at single-cell resolution. *Curr. Biol.* **21**, 1–11 (2011).

106. E. Bullmore, O. Sporns, The economy of brain network organization. *Nat. Rev. Neurosci.* **13**, 336–349 (2012).

107. C. I. Bargmann, E. Marder, From the connectome to brain function. *Nat. Methods* **10**, 483–490 (2013).

108. J. R. Cohen, M. D'Esposito, The segregation and integration of distinct brain networks and their relationship to cognition. *J. Neurosci.* **36**, 12083–12094 (2016).

109. M. Rubinov, O. Sporns, Complex network measures of brain connectivity: Uses and interpretations. *Neuroimage* **52**, 1059–1069 (2010).

110. O. Sporns, C. J. Honey, R. Kötter, Identification and classification of hubs in brain networks. *PLoS One* **2**, e1049 (2007).

111. J. D. Power, B. L. Schlaggar, C. N. Lessov-Schlaggar, S. E. Petersen, Evidence for hubs in human functional brain networks. *Neuron* **79**, 798–813 (2013).

112. M. Bastian, S. Heymann, M. Jacomy, "Gephi: An open source software for exploring and manipulating networks" in *International AAAI Conference on Weblogs and Social Media* (Association for the Advancement of Artificial Intelligence, 2009).

113. M. Jacomy, T. Venturini, S. Heymann, M. Bastian, ForceAtlas2, a continuous graph layout algorithm for handy network visualization designed for the Gephi software. *PLoS One* **9**, e98679 (2014).

NEUROSCIENCE

Kimbrough et al.

www.manaraa.com